SMART PARTS FABRICATION USING POWDER BED FUSION ADDITIVE MANUFACTURING TECHNOLOGIES

Mohammad Shojib Hossain[1,2] , Jose A. Gonzalez[1,3] , Ricardo Martinez Hernandez[2], Philip Morton[1,2] , Jorge Mireles[1,2] , Ahsan Choudhuri[2] , Yirong Lin[2] , and Ryan B. Wicker[1,2]

[1]W.M. Keck Center for 3D Innovation, The University of Texas at El Paso, TX 79968, USA
[2]Department of Mechanical Engineering, The University of Texas at El Paso, TX 79968, USA
[3]Department of Metallurgical, Materials and Biomedical Engineering, The University of Texas at El Paso, TX 79968, USA

Abstract

Metallic components with embedded sensors or smart parts can be a beneficial tool for monitoring harsh environments in the energy, biomedical, automotive, and aerospace industries. Smart parts maintain structural integrity with added functionality of sensing temperature, pressure, and structural health. A non-intrusive placement of a sensor in metallic components was developed using powder bed fusion additive manufacturing (AM). A paused build procedure was used to fabricate a proof of concept, a cylindrical shaped smart part using both electron beam melting (EBM) and selective laser melting (SLM) technologies. This paper focuses on the fabrication process and characterization of the smart part. A functional complex shaped energy system component, a smart injector was fabricated to demonstrate the applicability in harsh environments. The pressure and temperature sensing capabilities were tested using compressive cyclic loading and hot fire testing in a combustion chamber testing. A maximum sensing response of 3V was obtained for EBM fabricated smart part while applying compressive load. An image analysis based part positioning method was demonstrated for EBM technology that can be employed in other AM technologies to alleviate or completely remove misalignment in a paused build fabrication process.

Introduction

Additive manufacturing (AM) technology is advancing manufacturing of smart parts with embedded sensors, wires, electronic components, and multiple material in end use parts. The embedded piezoceramic sensor in a metallic component or smart part can be an effective way of obtaining real time performance temperature and pressure feedback. The energy industry can benefit from *in situ* process monitoring to improve efficiencies, in turn lowering emissions, and ensuring system safety of combustion processes. Surface contacts, adhesive based contacts, or drilled holes are typical surface placement methods for thermocouples and pressure sensors in energy system components. The surface or outer sensor placements can result in modification of part's design in turn affecting regular operation. For example, the aerodynamic performance or wind flow over a wind turbine can be affected by reducing aerodynamic properties due to design alterations. Moreover, harsh environments can negatively impact sensor life or cause unreliable readings. External thermocouples or pressure sensors can measure the external conditions, but not the inner condition of the components, within a combustion chamber for example. AM technology fabricates complex shaped parts in a layer-by-layer fashion that can be paused to embed sensor material in a desired location. Powder bed fusion (PBF) is a process category of AM technology

that uses precursor metal powder to create metallic components using an energy source specific to the technology (laser or electron beam) [1]. PBF process include direct metal laser sintering (DMLS), electron beam melting (EBM), selective laser melting (SLM), and selective laser sintering (SLS) technologies [2]. The three main aspects of the embedding process addressed in this paper are: 1) embedding technique of piezoceramic sensor material in metallic body, 2) sensor functionality as a pressure and temperature sensor, and 3) part positioning using image analysis technique. Smart parts were fabricated using EBM and SLM.

Piezoceramic sensor works as a pressure sensor when a dynamic load is applied. The piezoelectric effect creates an electric charge in the presence of applied force on the piezoceramic material and vice versa [3]. The electric response can be converted to values of strain, pressure, and force after proper calibration [4]. The pyroelectric effect creates electrical charge in response to heat flux, charge/heat flux coupling is dependent on polarization of the material [5]. Lead zirconate titanate (PZT) shows both piezoelectric and pyroelectric effect, making PZT an excellent choice for both pressure and temperature sensing material. Li *et al.* demonstrated embedding of thermo-mechanical sensors within a metallic structure using shape deposition modeling (SDM) technology [6]. Delamination between of the layers where the embedding took place was observed in the SDM process. Aguilera *et al.* worked on fabrication process of an electromechanical device that required the embedding of electronic components using fused deposition modeling (FDM) technology [7]. The use of thermoplastic material restricts the applications in elevated temperatures applications. Pille worked on embedding of piezo sensor and RFID transponder inside of die cast zinc alloy parts [8]. Rai *et al.* showed embedding technique of thermocouples and strain gauges using SLS process, where the operating temperature reached ~170^{o} C [9]. The high operating temperature fabrication process of PBF technologies (for example, EBM systems typically run at >700^{o} C) limit the choice of sensor material for embedding purposes. Any kind of protective layer or insulating material will be required to withstand high fabrication temperature of PBF technologies.

Another aspect of embedding technique is registration of the fabricated parts after embedding process. The embedding process often requires the base part to be removed from the EBM machine. SLM technologies, the build platform is secured using fixed position bolts which minimizes placement error. After the embedding process using the SLM technologies, the start plate can be placed in its previous position and the fabrication is continued. On the other hand, start plate position in build platform cannot be referenced using EBM technology, the start plate is placed directly on the powder bed with no securement. Thus, alignment of the part is essential to continue fabrication after embedding the sensor package due to the part and start plate movement. Touch probes and laser scanners are common referencing or positioning tools typically used in computer numerical control (CNC) machining, tooling equipment, and measurement devices. Persson *et al.* demonstrated the use of laser scanner and touch probe scanner for dental surface topography measurements that showed a repeatability of the scanners within 10 μm [10]. Park *et al.* showed a coordinate measuring machine (CMM) with force sensing touch probe and found a contact point error of ±10 μm [11]. Although the measurements using touch probe and laser scanner provides high accuracy measurements, the installation of such devices require additional or special installation space. Moreover, the EBM machine runs at a high temperature (>700^{o} C) that requires high temperature electronics and instrumentation to survive the build environment. The thermal expansion of the part needs to be accounted in the part positioning

calculation that can be avoided by performing real time monitoring system. An infrared thermography (IR) based image analysis is a plausible solution that meets all requirements for EBM fabrication, it is mounted externally in order to limit installation space, temperature exposure, and provides instantaneous monitoring. The image analysis technique utilizes a real time monitoring system so that the thermal expansion issue can be neglected.

The work presented here showed the fabrication process of cylindrical shaped smart parts using SLM and EBM technologies. The sensor capability was demonstrated using a compression-compression loading test. A smart injector was fabricated using SLM technologies to show the capabilities of fabricating complex shaped part and performing component level testing. The smart injector was tested in a combustion chamber to show sensor responses in correspondence to temperatures changes. The part positioning was demonstrated using a cylinder and a rectangular prism to demonstrate the ability to align both linear and angular alignment of the part. The developed process shown here can be implemented for complex shaped parts to attain multi-functional smart structures for engineering applications in the field of energy systems, aerospace industries, biomedical implants, and auto industries.

Materials

The smart part is made up of several components, a schematic diagram of the assembly (Figure 1) is shown, Figure 1(a) shows an exploded view of the sensor assembly and Figure 1(b) shows the final assembly. The sensor assembly consists of piezoelectric ceramic material, electrodes, and insulating material. In this experiment, PZT was used as a sensor material for its high piezoelectric coefficient (d_{33} value ~400 pC/N) [12]. Tungsten was selected as the electrode

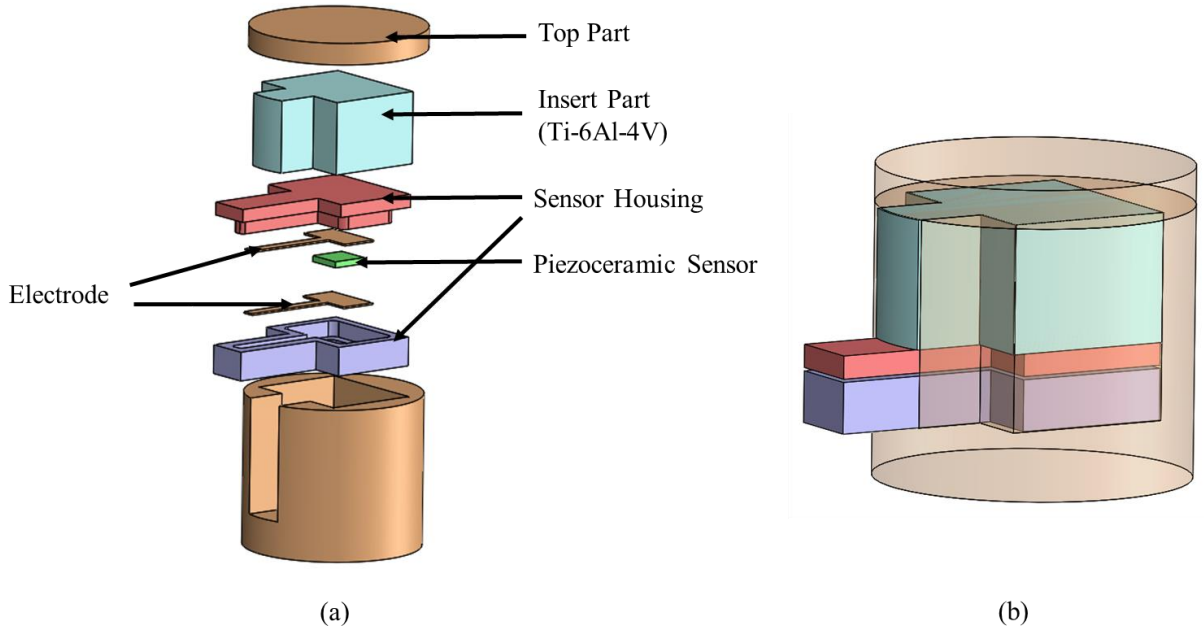

Figure 1. Schematic diagram of smart parts, (a) components of sensor assembly and (b) assembled diagram

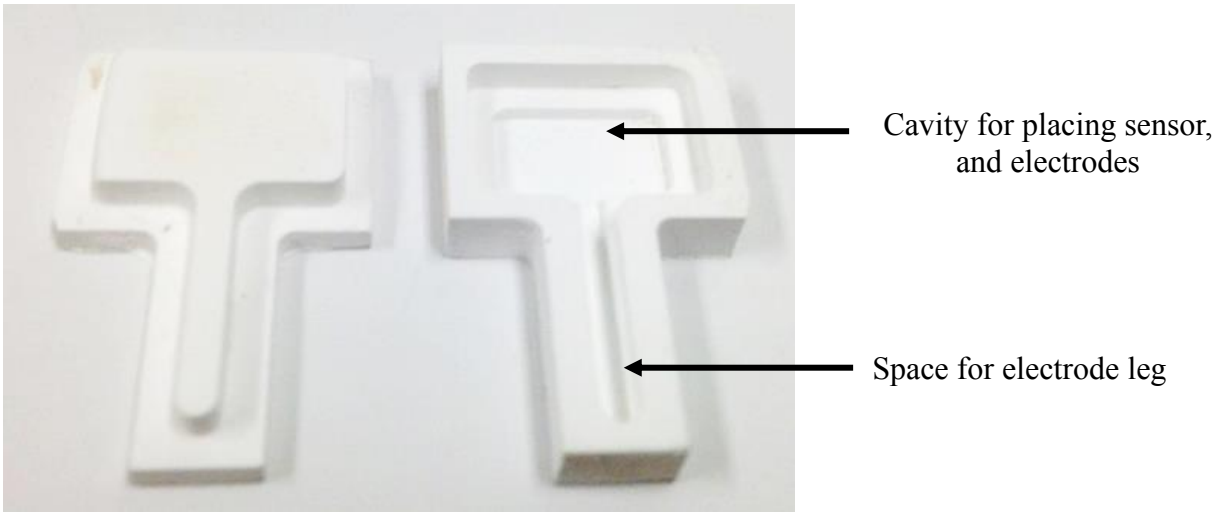

Figure 2. Alumina housing for protecting the sensor material

material for its high vaporization temperature [13]. Alumina was used as insulating material to isolate the sensor material from the metallic body. Additionally, a housing was fabricated using a CNC Mini Mill 2 (HAAS Automatic Inc., CA) from the alumina (shown in Figure 2) and used to protect the sensor components from metallization during EBM processing. Metallization occurs in EBM due to the high temperatures and high vacuum environment, causing metal to vaporization and coat surfaces. No metallization occurs during SLM fabrication requiring only alumina plate to be used as insulators for the smart parts. The extended portion of the sensor housing was broken off after the fabrication process was finished. An isolation cup was implemented during fabrication of EBM smart parts to prevent metal powder from short circuiting the sensor assembly. The structure of the smart parts was fabricated using Ti-6Al-4V and Inconel 625 powder for EBM and SLM systems, respectively. Parameters for both materials are commercially available and both materials are well suited for energy industry components.

Fabrication Process

In this paper, the embedding process of PZT sensor material was explored using both PBF technologies, EBM and SLM. The fabrication procedure involves the insertion of sensor assembly into the metallic structure at a specific height while PBF process is paused, and subsequently continuing the fabrication process. The part included a cavity to house the sensor, after sensor placement a cap is included to cover the sensor and provide a surface to resume fabrication. The fabrication steps differs based on the PBF technology used. The EBM "stop and go" process consists of six steps and are shown in Figure 3. The process starts with fabricating the bottom and insert part (step 1), the insert part is necessary to cap and hold the sensor assembly and create a planar surface to allow fabrication to proceed. Step 2 is to embed sensor assembly within the part's cavity, using a ceramic housing and insert part. Next, step 3 requires machining of mask plate to create a planar surface for fabrication, align the part when the process is resumed, and reduce any powder charging which results in a smoking event during the fabrication process [14]. Then, the part containing the sensor assembly is placed in the masked to prepare to resume fabrication in step 4. The top of the smart part is fabricated when the process continues (step 5) and the smart part is complete after removal from the mask plate in (step 6).

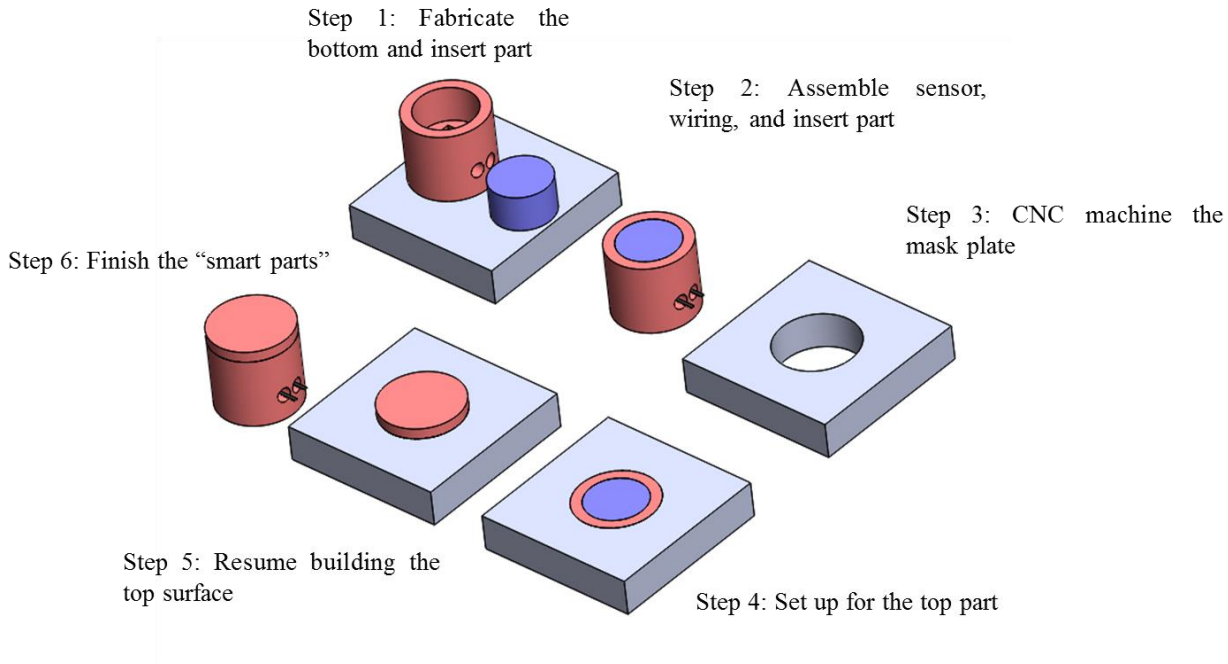

Figure 3. "Stop and go" process to fabricate smart parts using EBM technology

The smart part fabrication process or "stop and go" using SLM technology requires five steps and are shown in Figure 4. In comparison to EBM fabrication, no mask plate is required, and the bottom part is bonded to the start plate and never removed during the stop and go process. As a result, the part can be aligned using the build platform fixture bolts which provides high placement repeatable. The steps for fabrication are as follows, step 1 is to fabricate the insert part, step 2 fabricate the bottom part on a separate build platform, step 3 the sensor assembly and insert part are stacked together and placed in the cavity, step 4 resumes the SLM fabrication process, and step 5 the smart part is completed.

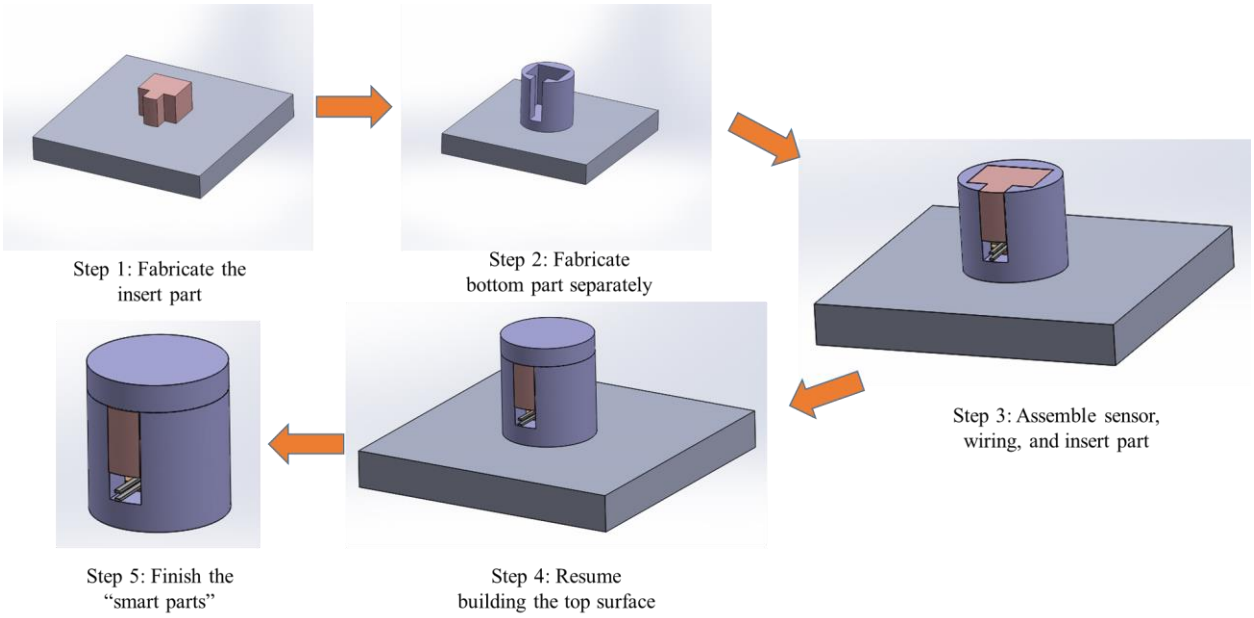

Figure 4. "Stop and go" process to fabricate smart parts using SLM technology

Part Positioning Methodology

A part positioning technique is required for EBM fabrication of the smarts parts, but can be applied to other technologies where realignment is required. After removing the part from the build platform, the part cannot be placed in its previous position, hence part positioning becomes necessary. The part positioning algorithm was developed using MATLAB (MathWorks, Natick, MA) based on image analysis techniques to find the centroid location and angular rotation of the part. A cylindrical part and a rectangular prism were fabricated to demonstrate both linear and angular alignment using image analysis to calculate the misalignment and calculate the origin. A FLIR SC645 (FLIR Systems Inc., Wilsonville, OR) infrared (IR) camera was used to obtain images before and after the embedding process which was operated by a virtual instrument using LABVIEW (National Instruments, Austin, TX). The translation and rotation of the part can be calculated by comparing binary images of the part before removal from the EBM system and after replacement. In this analysis, an IR image is converted into a binary image, the part is designated as 1 (white) and the powder as 0 (black). From a binary image, the centroid can be calculated using total pixel value of the part [15]. For binary image, B[i,j], the centroid can be calculated by,

$$\bar{x} = \frac{\sum_{i=0}^{c-1} \sum_{j=0}^{r-1} jB[i,j]}{A} \quad (1)$$

$$\bar{y} = \frac{\sum_{i=0}^{c-1} \sum_{j=0}^{r-1} iB[i,j]}{A} \quad (2)$$

Where $\bar{x}$ and $\bar{y}$ are the centroid pixel location of the measured part, and A is the area of the part calculate from the image.

The binary image is shown in Figure 5a, and the calculated centroid is shown in Figure 5b as a blue dot. The centroid was calculated using equations 1 and 2, were used to identify the position before and after embedding. Next, the linear displacement was calculated using the difference of the centroid pixel locations of the images from the before and after images. Calculating the new part position is done by using the original EBM origin position (P_1, Q_1), the measured centroid pixel position ($X_{centroid,1}$, $Y_{centroid,1}$), and the new centroid pixel position ($X_{centroid,2}$, $Y_{centroid,2}$) after repositioning the part. The center beam location after repositioning, (P_2, Q_2), can be calculated using the following equations,

$$P_2 = P_1 + \alpha \times (X_{centroid,2} - X_{centroid,1}) \quad (4)$$

$$Q_2 = Q_1 + \alpha \times (Y_{centroid,2} - Y_{centroid,1}) \quad (5)$$

A conversion coefficient, α, was used to convert pixel to mm values. The conversion coefficient was calculated using a known distance of four cylinders in the build platform. Five images at different layers were considered for calculation and the average was used to obtain α value.

The edge locations of the part was obtained using Canny edge detection technique [16]. The coordinates of the edges were used to calculate the slopes of the edges. Using the slope and an inverse tangent function the angle was calculated. The angular displacement (R) of the part was calculated using the angle before the pause (R1) and the angle after the pause (R2) and is shown in the following equation,

$$R = R1 - R2 \quad (10)$$

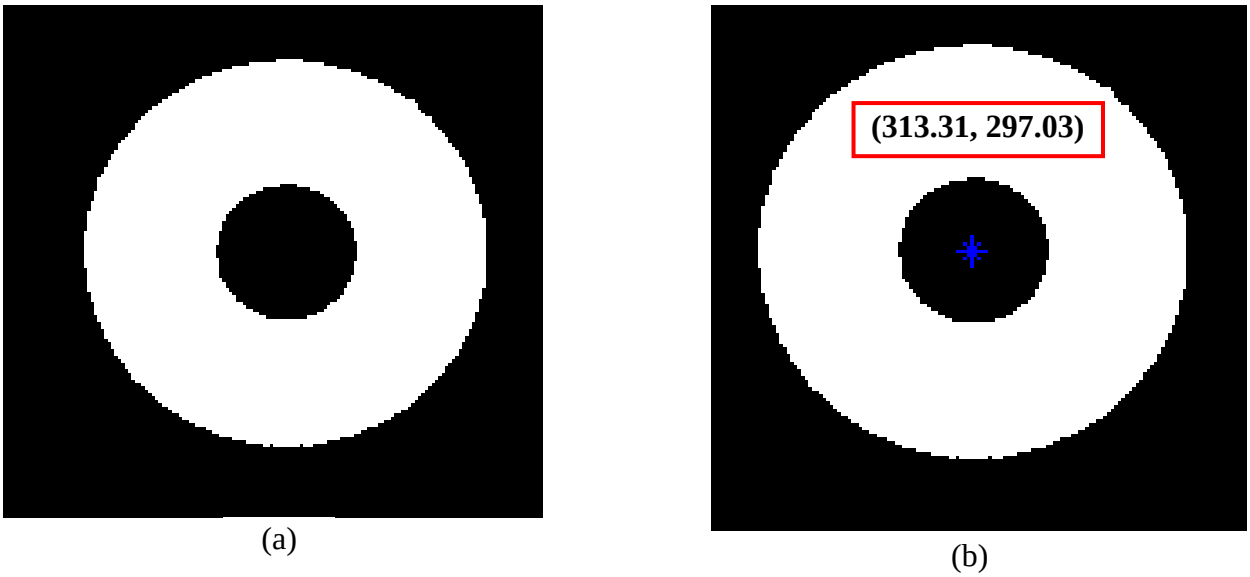

(a) (b)

Figure 5. Centroid location calculation using a binary image. The part is shown in white color. (a) Conversion of binary image and (b) detection of centroid (denoted using blue asterisk) and centroid pixel location is shown in red bounding box

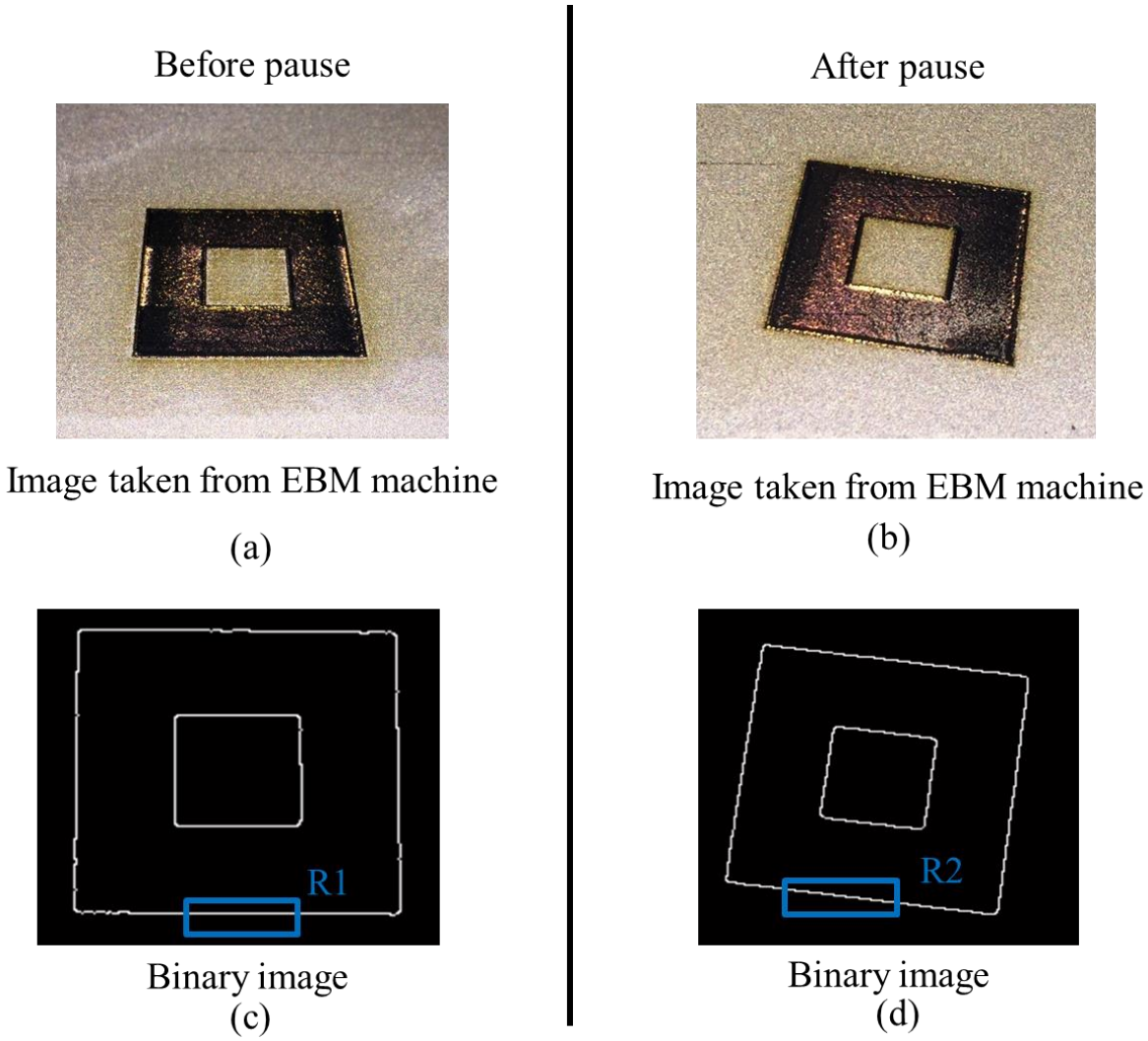

Figure 6. Edge detection and angle measurement for angular displacement. (a) & (b) optical image taken from EBM build platform of before and after pausing the system, respectively, and (c) & (d) binary image of the corresponding part of before and after pausing the system, respectively. The blue bounding box represents the edge considered for angle calculation and R1 and R2 are the calculated angle of the corresponding edges. The optical images show the part's positions within the build platform but are not involved in image analysis calculations

Edge detection and angle measurements were taken from the images shown in Figure 6. Figure 6 (a) and 6 (c) depicts the optical and binary image of before pausing the system, and Figure 6 (b) and 6 (d) depicts the optical and binary image of after pausing the system, respectively. Figure 6 (c) and Figure 6 (d) demonstrates the corresponding angle R1 and R2. The obtained angular displacement R was applied in the CAD model by rotating the entire part in the x-y coordinate systems, rotation cannot be changed through the machine's interface.

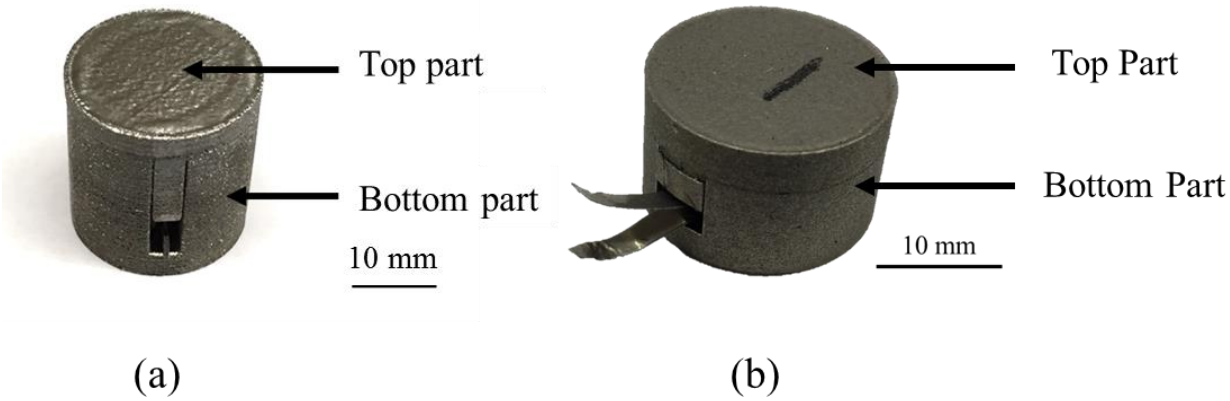

Figure 7. Smart parts fabricated using (a) EBM and (b) SLM technology

Results and Discussion

Smart Parts:

Two versions of the smart parts were fabricated, EBM (Figure 7a), and SLM (Figure 7b), both smart parts contain PZT sensors, electrodes, and insulating material as shown in Figure 1. The sensor housing has been broken as shown in Figure 7 (a) and Figure 7 (b) shows the SLM fabricated smart part, where alumina plates were used. After fabrication every smart part was evaluated by testing for open circuit condition between the sensor electrodes using a SPERRY DM-4400A digital multi-meter (SPERRY Instruments, Menomonee Falls, WI). An additional step of re-poling was required for the PZT sensor to recover the piezoelectric coefficient (d_{33}) [17].

Force Sensing:

A compression-compression test was performed to evaluate the force sensing capability of the EBM fabricated smart part. A flat end cylindrical fixture and load concentrator (Figure 8) was used for testing. The load concentrator transferred the load to the center of the smart part, where

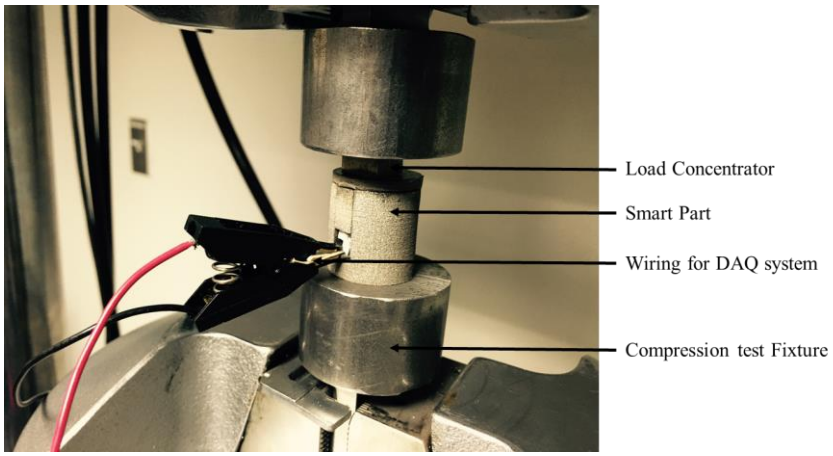

Figure 8. Force sensing test set up of smart part

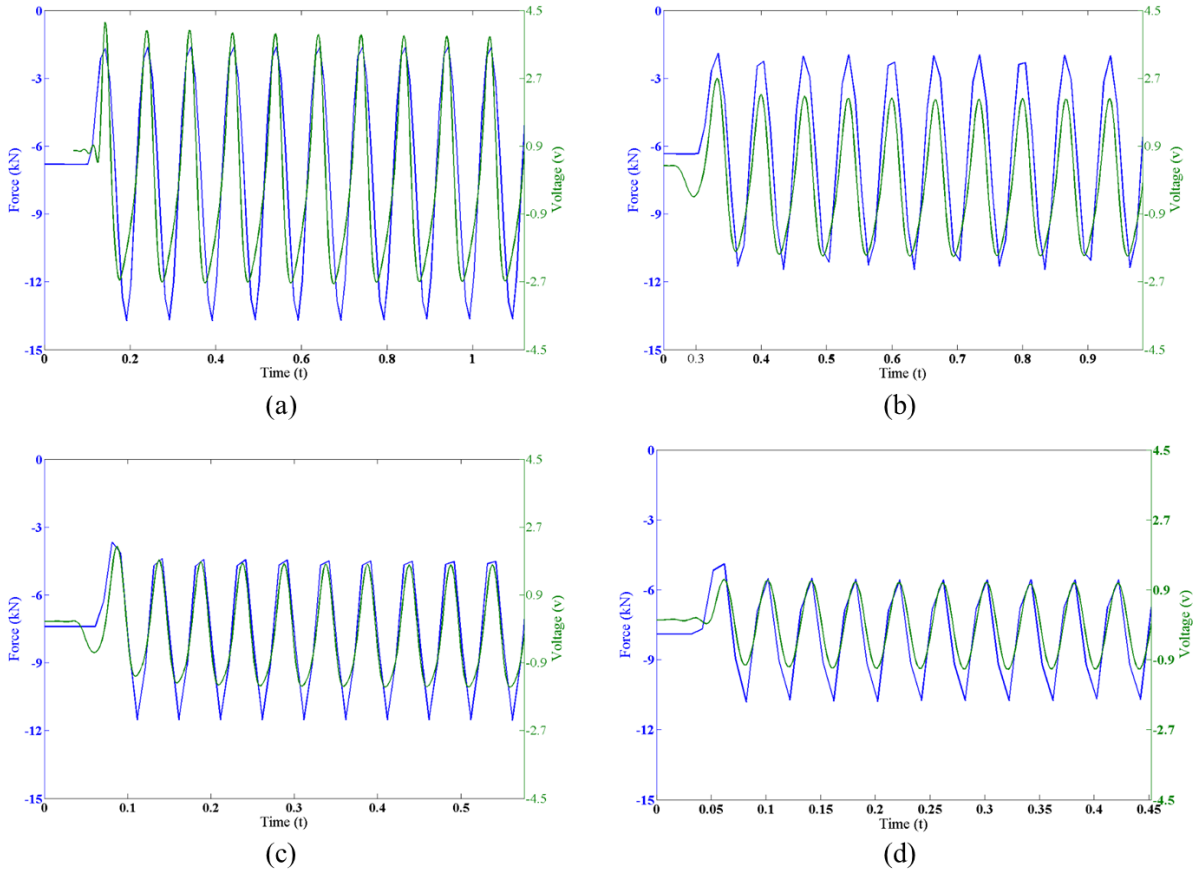

Figure 9. Voltage response obtained from smart part in accordance to applied force at frequencies of (a) 10 Hz, (b) 15 Hz, (c) 20 Hz, and (d) 25 Hz

the PZT sensor material resides. The testing was performed using a MTS Landmark Servohydraulic test system (Eden Prairie, MN). The test specimen was compressed initially at ~0.25 mm and oscillated ± 0.1 mm using four different frequencies of 10 Hz, 15 Hz, 20 Hz, and 25 Hz. The voltage responses were recorded using a NI PCI-6621 DAQ system (National Instruments, Austin, TX), and plotted against time. Figure 9 shows the PZT voltage response under the four frequencies corresponding to the applied force. The voltage response results show the functionality of the smart parts as a force/pressure sensor. The sensing voltage for different frequencies showed good agreement with the applied force on the smart parts. A calibration method can be developed to evaluate the smart part's operation for engineering applications.

Smart Injector:

A smart injector was fabricated to demonstrate the capability of PBF "stop and go" manufacturing to fabricate complex shapes, shown in Figure 10. Two sensor assemblies were embedded inside the metallic body, the electrodes of the sensors are visible in Figure 10. The injector was tested in a combustion chamber (Figure 11) to compare the sensor temperature reading to a surface thermocouple. The flame created at the tip is shown in Figure 11 (a) and the corresponding sensor response due to temperatures change is shown in Figure 11 (b).

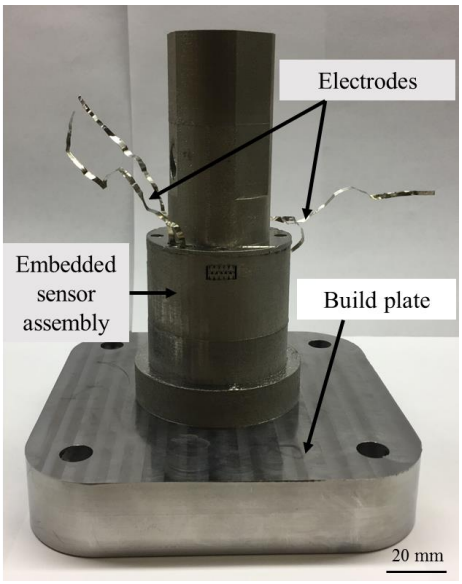

Figure 10. Smart injector fabricated using SLM technology

Alignment Results:

Parts fabricated with the "stop and go" are shown in Figure 12, a cylinder and a rectangular prism that were paused mid build, moved arbitrarily, and aligned using image analysis. Different geometries were used to evaluate both motion types, the cylinder only used translation and the rectangular prism required both translation and rotation. The misalignment was measured using integrated laser measurement system from an OGP SmartScope Flash 250 (OGP, Rochester, NY), shown in Figure 13 for both test coupons. Points spaced 0.025mm were used to obtain 16 line scan measurements for the cylindrical part and resulted in a maximum average misalignment of 0.15 mm. The rectangular prism was measured using three points per side of the top and bottom section (Figure 13(b)), eight edges were used for the misalignment calculation. A maximum average misalignment of 0.87 mm was obtained for the rectangular prism.

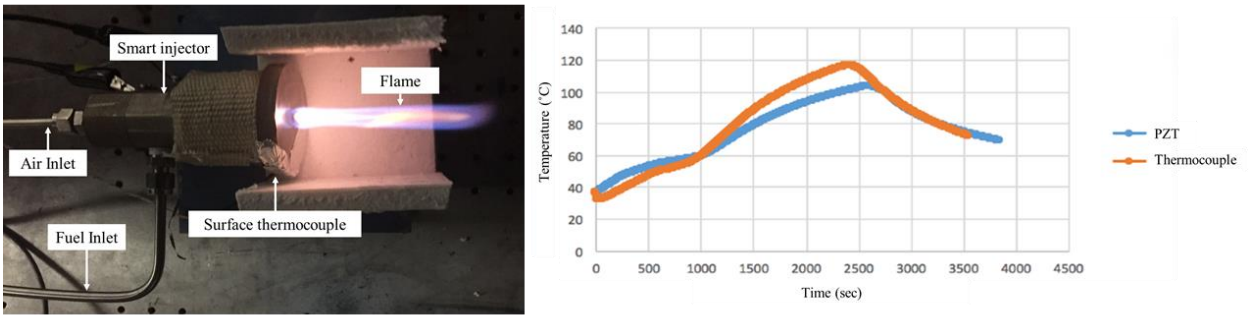

Figure 11. Smart injector testing (a) combustion chamber test set-up and (b) temperature sensing response and surface thermocouple results

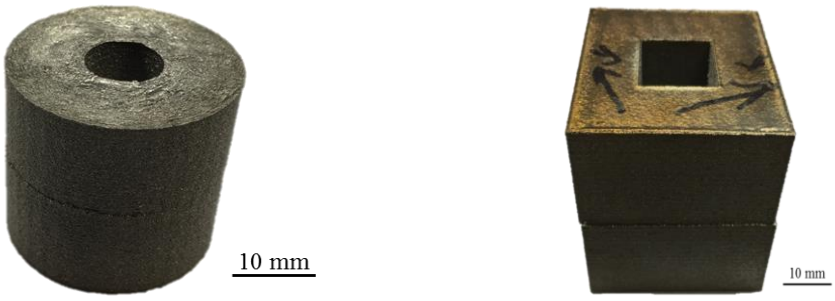

(a) (b)

Figure 12. Parts aligned using image analysis based part positioning technique, (a) cylindrical part and (b) rectangular prism

Conclusion

The work presented here showed the embedding and alignment techniques to fabricate smart parts with embedded piezoceramic sensor material in PBF technologies. This research demonstrated the fabrication process of a complex shaped energy system component, a smart injector. Embedding sensor can prolong the life cycle when used in harsh/hard-to-reach environments and provide valuable process data to improve efficiency. Monitoring position for realignment is critical to prevent any registration or alignment errors during fabrication. PBF technology provides opportunity to fabricate, parts containing embedded sensor material at any

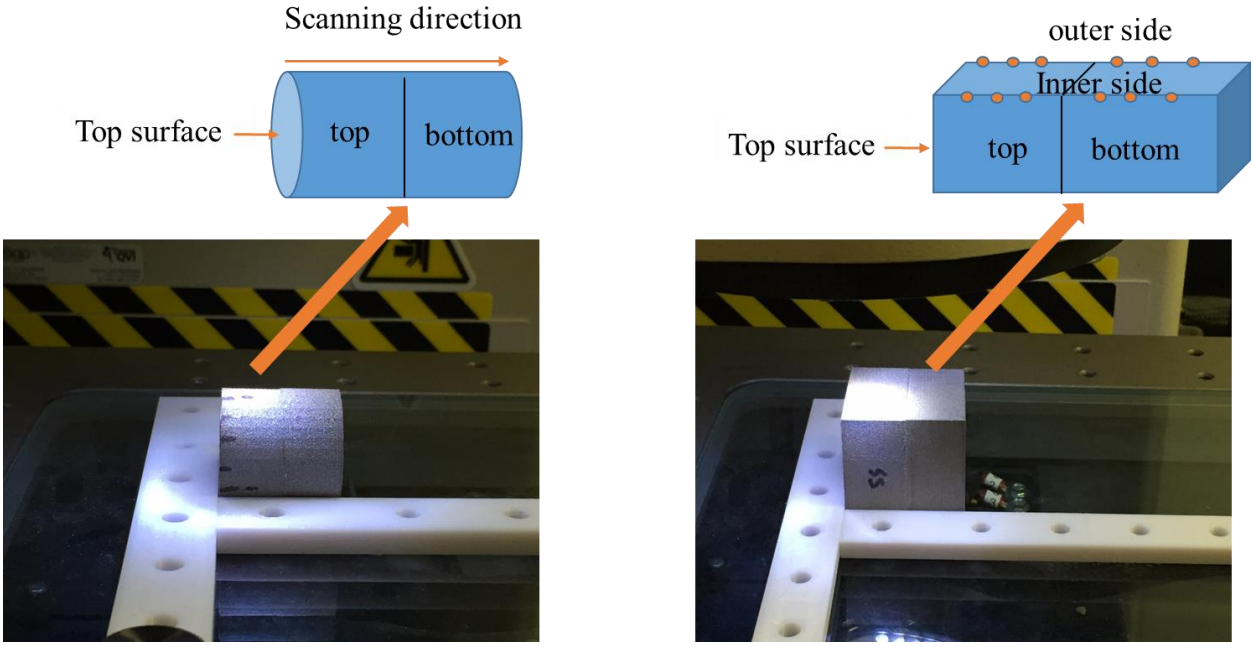

(a) (b)

Figure 13. Misalignment measurement (a) cylindrical part and (b) rectangular prism. The white bar was used to aligning the part in the platform

desired height or position in complex parts. Moreover, the "stop and go" process gives the opportunity to fabricate complex shaped parts without altering a part's geometry or structural integrity. To enable the "stop and go" manufacturing, image analysis techniques were developed to minimize repositioning errors for both translational and rotational errors when replacing the part in the EBM machine. Furthermore, methods described herein can be a pathway for achieving multi-functional and multi-material end use parts using PBF based AM technologies.

Acknowledgements

The research was performed at The University of Texas at El Paso (UTEP) in the W.M. Keck Center for 3D Innovation, providing access to the state-of-the-art facilities and equipment. The research was supported, in part, by the U.S. Department of Energy (DOE-NETL) through award number DE-FE0012321. Any findings, opinions, conclusions, or suggestions herein are those of the authors, and do not necessarily reflect the views of the DOE or any other funding source or agency.

References

[1] H. Gong *et al*, "Analysis of defect generation in Ti–6Al–4V parts made using powder bed fusion additive manufacturing processes," *Additive Manufacturing,* vol. 1, pp. 87-98, 2014.

[2] I. Gibson, D. W. Rosen and B. Stucker, *Additive Manufacturing Technologies.* 2010*238*.

[3] A. Arnau, *Piezoelectric Transducers and Applications.* 2004*2004*.

[4] J. Sirohi and I. Chopra, "Fundamental understanding of piezoelectric strain sensors," *J Intell Mater Syst Struct,* vol. 11, *(4),* pp. 246-257, 2000.

[5] J. G. Webster and H. Eren, *Measurement, Instrumentation, and Sensors Handbook: Spatial, Mechanical, Thermal, and Radiation Measurement.* 2014.

[6] X. C. Li, A. Golnas and F. B. Prinz, "Shape deposition manufacturing of smart metallic structures with embedded sensors," in *PROCEEDINGS-SPIE THE INTERNATIONAL SOCIETY FOR OPTICAL ENGINEERING,* 2000.

[7] E. Aguilera *et al*, "3D printing of electro mechanical systems," in *Proceedings of the Solid Freeform Fabrication Symposium,* 2013.

[8] C. Pille, "In-process-embedding of piezo sensors and RFID transponders into cast parts for autonomous manufacturing logistics," *Smart Systems Integration,* pp. 1-10, 2010.

[9] R. Rai, M. Campbell and K. Wood, "Extracting product performance by embedding sensors in SFF prototypes," in *Proceedings of International Solid Freeform Fabrication Symposium, Austin, Texas,* 2004.

[10] A. Persson *et al*, "A three-dimensional evaluation of a laser scanner and a touch-probe scanner," *J. Prosthet. Dent.*, vol. 95, *(3)*, pp. 194-200, 2006.

[11] J. Park, K. Kwon and N. Cho, "Development of a coordinate measuring machine (CMM) touch probe using a multi-axis force sensor," *Measurement Science and Technology*, vol. 17, *(9)*, pp. 2380, 2006.

[12] S. Zhang *et al*, "Piezoelectric materials for high power, high temperature applications," *Mater Lett*, vol. 59, *(27)*, pp. 3471-3475, 2005.

[13] I. Langmuir, "The vapor pressure of metallic tungsten," *Physical Review*, vol. 2, *(5)*, pp. 329, 1913.

[14] H. Tang *et al*, "Effect of powder reuse times on additive manufacturing of Ti-6Al-4V by selective electron beam melting," *JOM*, vol. 67, *(3)*, pp. 555-563, 2015.

[15] M. Sonka, V. Hlavac and R. Boyle, *Image Processing, Analysis, and Machine Vision.* 2014.

[16] J. Canny, "A computational approach to edge detection," *IEEE Trans. Pattern Anal. Mach. Intell., (6)*, pp. 679-698, 1986.

[17] A. D. Prewitt, *Effects of the Poling Process on Dielectric, Piezoelectric, and Ferroelectric Properties of Lead Zirconate Titanate.* 2012.